incomplete. VLA observations to determine the nature of potential SNR candidates are in progress.

We end with an observation. It is usually assumed, for the purpose of identification of counterparts, that only the total area of the localization matters. But as Equation (1) shows, a localization with a very long axis is undesirable in two situations: (1) extended counterparts (for example, SNRs as discussed above) or (2) when clustering statistics of the bursts are expected to provide crucial clues (for cosmological models, for instance). In the second case, the clustering statistics will be limited to angular scales set by the long axis. Large-area X-ray monitors with masks have the advantage of providing circular localizations with acceptable areas. □

Received 1 June; accepted 16 July 1993.

1. Mazets, E. P., Golenetskii, S. V., Guryan, Yu A. & Ilyinskii, V. N. *Astrophys. Space Sci.* **84,** 173–189 (1982).
2. Laros, J. G. *et al. Astrophys. J.* **320,** L111–L115 (1987).
3. Atteia, J.-L. *et al. Astrophys. J.* **320,** L105–L110 (1987).
4. Kouveliotou, C. *et al. Astrophys. J.* **322,** L21–L25 (1987).
5. Norris, J. P., Hertz, P., Wood, K. S. & Kouveliotou, C. *Astrophys. J.* **366,** 240–252 (1991).
6. Cline, T. L. *et al. Astrophys. J.* **255,** L45–L48 (1982).
7. Shaver, P. A. & Goss, W. M. *Aust. J. Phys. astrophys. Suppl.* **14,** 133–196 (1970).
8. Green, D. A. *Publs. Astr. Soc. Pacif.* **103,** 209–220 (1991).
9. Felten, J. E. *Proc. 17th Int. Cosmic Ray Conf. Paris* **42,** 52–55 (1981).
10. Cline, T. *et al. Proc. 21st Int. Cosmic Ray Conf.* **12,** 19–38 (1990).
11. Higdon, J. C. & Lingenfelter, R. E. *Ann. Rev. Astr. Astrophys.* **28,** 401–436 (1990).
12. Shaver, P. A. & Goss, W. M., *Aust. J. Phys. astrophys. Suppl.* **14,** 77–131 (1970).
13. Reich, W., Fürst, E., Steffen, P., Reif, K. & Haslam, C. G. T. *Astr. Astrophys. Suppl. Ser.* **58,** 197–248 (1984).
14. Neff, S. G., Hutchings, J. B. & Gower, A. C. *Astr. J.* **97,** 1291–1305 (1990).
15. Milne, D. K. *Aust. J. Phys.* **32,** 83–92 (1979).
16. Hurley, K. *et al. Astr. Astrophys. Suppl. Ser.* **97,** 39–41 (1993).
17. Braun, R., Goss, W. M. & Lyne, A. G. *Astrophys. J.* **340,** 355–361 (1989).
18. Vancura, O., Blair, W. P., Long, K. S. & Raymond, J. C. *Astrophys. J.* **394,** 158–173 (1992).
19. van den Bergh, S. & Tammann, G. A. *A. Rev. Astr. Astrophys.* **29,** 363–407 (1991).
20. Narayan, R. *Astrophys. J.* **319,** 162–179 (1987).
21. Duncan, R. C. & Thompson, C. *Astrophys. J.* **392,** L9–L13 (1992).
22. Paczyński, B. *Acta Astronomica* (submitted).
23. Melia, F. & Fatuzzo, M. *Astrophys. J.* **408,** L9–L12 (1993).
24. Kouveliotou, C. *et al. Nature* **362,** 728–730 (1993).

ACKNOWLEDGEMENTS. S.R.K. is indebted to T. Murakami for getting him interested in gamma ray bursters. S.R.K. thanks H. Komiya for suggesting the idea leading to equation (1), T. Murakami and W. Deich for discussions, and Y. Tanaka and ISAS for hospitality under the ISAS Visiting Professorship programme. We thank the librarians at Centre de Données astronomiques de Strasbourg, France for maintaining the SIMBAD database and to the National Radio Astronomy Observatory for initiating and operating the VLA archival program. S.R.K. is supported in part by NASA, the National Science Foundation (NSF) and the Packard Foundation. D.A.F. is supported by a NRAO Jansky postdoctoral research associateship. The VLA is operated by Associated Universities Inc. under a cooperative agreement with the N.S.F.

Entropy-driven formation of a superlattice in a hard-sphere binary mixture

M. D. Eldridge*, P. A. Madden* & D. Frenkel†

* Physical Chemistry Laboratory, Oxford University, South Parks Road, Oxford OX1 3QZ, UK
† FOM-Institute for Atomic and Molecular Physics, Kruislaan 407, NL-1098 SJ Amsterdam, The Netherlands

A MIXTURE of two dissimilar species (A and B) may freeze to form a substitutionally ordered crystal, the structure of which can vary from a lattice with only a few atoms per unit cell to a complex 'superlattice'. For example, a mixture of sodium and zinc can form a solid with the AB_{13} structure with 112 atoms per unit cell[1] (Fig. 1*a*). One might suspect that very specific energetic interactions are needed to stabilize a structure as complex as this. But recent experiments[2,3] show that the AB_{13} structure is also formed in mixtures of spherical colloidal particles with different diameters, which interact only via simple repulsive potentials. This raises the possibility that the formation of an AB_{13} superlattice might be supported by entropic effects alone. To investigate this possibility, we present here computer simulations of a binary mixture of hard spheres. Our calculations show that entropy alone is indeed sufficient to stabilize the AB_{13} phase, and that the full phase diagram of this system is surprisingly complex. Our results also suggest that vitrification or slow crystal nucleation in experimental studies of colloidal hard spheres can prevent the formation of equilibrium phases.

To predict the phase diagram of a binary mixture by computer simulation, we must determine the Gibbs free energies of all competing phases as a function of the external pressure (see, for example, ref. 4). On the basis of space-filling arguments[5], for diameter ratios ($\alpha = \sigma_B/\sigma_A$) in the range 0.5–0.8, the following phases may be expected to occur in a mixture of hard spheres: pure face-centred-cubic (f.c.c.) crystals of either component (A and B), the AB_{13} (Fig. 1*a*) and AB_2 (Fig. 1*b*) lattices, and the binary fluid (F). If a given structure has a very high volume fraction at close-packing (φ_{cp}), then at lower densities the constituent particles will have a large free volume in which to move and hence a high translational entropy. Murray and Sanders showed[5] that for $0.5 \leqslant \alpha \leqslant 0.8$, φ_{cp} is appreciably higher for AB_{13}

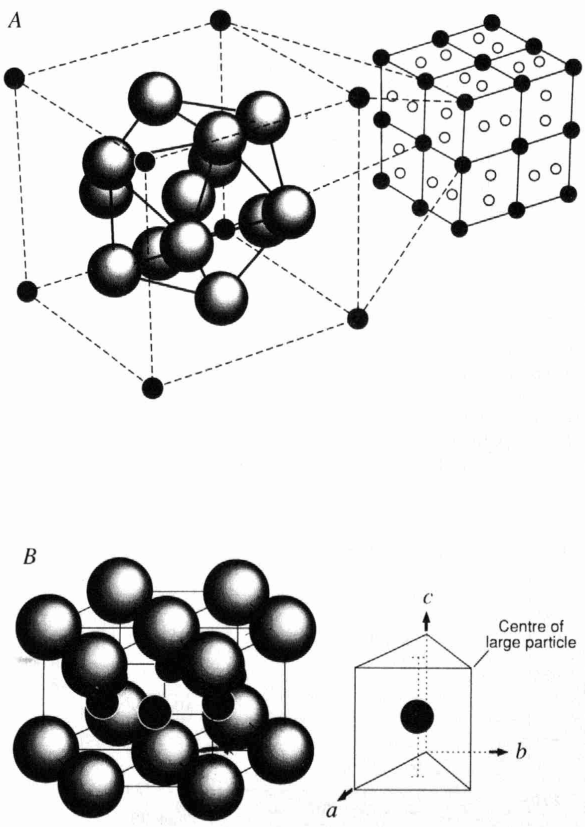

FIG. 1 *A*, The AB_{13} structure consists of body-centred icosahedral clusters of 13 B particles contained within simple cubic subcells of the larger component (A). The full unit cell (112 atoms) consists of eight subcells with neighbouring icosahedra alternating in orientation by $\pi/2$. *B*, The AB_2 structure is made up of alternating hexagonal layers of the small and large particles. The large particles (A) form close-packed layers aligning directly above each other along the c axis, while the small particles (B) occupy trigonal prismatic sites between these layers and form planar hexagonal rings resembling the carbon layers in graphite.

and AB_2 than for any other binary crystal structure. The maximum packing fraction of these mixed crystals is, however, comparable to that of the pure A and B phases ($\varphi_{cp} = 0.7405$). For α above 0.85 a random alloy with f.c.c. structure is known to be stable[6,7] and for small values of $\alpha (\lesssim 0.5)$ a range of interstitial structures (for example NaCl) might be expected to be stable, again on space-filling grounds.

To compute the Gibbs free energy of the possible phases of the mixture, we use a numerical technique called 'thermodynamic integration' (see for example ref. 8). In such calculations, one computes the reversible work needed to transform the phase under consideration into a state of known free energy. To compute the free energy of the binary fluid, we compute the reversible work needed to compress the fluid mixture from zero density (the ideal gas) to the required packing fraction. We have used the semi-empirical expression of Mansoori *et al.*[9] for the binary fluid equation-of-state, to facilitate such a calculation. Integration from the dilute gas cannot be used for solids, however, because of pronounced hysteresis on encountering the freezing transition. Instead we have used the method of Frenkel and Ladd[10], taking the reference state (of known free energy, F) to be the corresponding Einstein crystal, that is the same crystallographic structure with the particles bound to lattice sites by harmonic springs. These calculations have been described in detail elsewhere[11,12].

Figure 2 shows the reduced-pressure/composition (P^*/X) phase diagram for a diameter ratio, $\alpha = 0.58$. At low densities only the binary fluid is stable. However, for compositions $X \lesssim 0.9$, as the pressure is increased there is a tendency for f.c.c. solid A (large spheres) to be precipitated. At higher pressures still, the crystal structure AB_2 becomes stable in coexistence with either solid A or fluid, and at even greater pressures the AB_{13} superlattice is thermodynamically stable for compositions around its stoichiometric value, $X = 13/14$.

One could still argue that specific energetic contributions (to the effective interatomic interactions) may be responsible for the formation of AB_{13} and AB_2 structures in metallic[1] and molecular[13–15] mixtures or even in charge-stabilized colloids[16,17]. For hard-particle systems however, the only non-ideal contributions to the free energy are entropic in origin. Hence, we find that entropy, normally regarded as a driving force for disorder, is responsible for the formation of crystal structures with very complex order.

In the experiments of Bartlett *et al.*[2,3] the total volume accessible to the colloidal mixture is set by the suspending fluid. Hence, in order to compare our simulations with these experiments, it is more convenient to compute the phase diagram of the mixture at constant total volume. Such a representation of the phase diagram is shown in Fig. 3 where, following ref. 18, we use the partial packing fraction of small spheres (φ_B) and large spheres (φ_A) as the independent coordinates. A notable feature of this representation is the large amount of (φ_B, φ_A)-phase space occupied by triangular eutectic (three-phase) regions. In the P–X diagram, these eutectics were only represented by points, in accordance with the Gibbs phase rule. The ratio of the volumes of the phases participating in this three-phase coexistence is equal to the ratio of the areas of the three internal triangles formed between the point considered and the vertices of the three-phase region[18].

In Fig. 3, we have indicated the compositions of the suspensions for which Bartlett *et al.*[3] observed the formation of solid phases. The symbols denote the phases they identified from the light-scattering Bragg peaks. In general terms their observations agree well with our thermodynamic phase diagram. The freezing line is well located. In addition, the phase diagram clearly shows why the formation of AB_2 crystals at $X_B = 2/3$ did not occur at the packing fractions reached in the experiments, an observation highlighted by Bartlett *et al.*[3]

The most striking difference between simulation and experiment is that Bartlett *et al.*[3] did not observe formation of solid A at compositions for which it is the thermodynamically favoured phase. At the composition corresponding to the AB_2 stoichiometry, an amorphous solid appeared instead of A. For compositions corresponding to AB_4 and AB_6, solid AB_2 and fluid (F) was observed, as if the system had avoided the lowest thermodynamic state (A + F) and settled into the neighbouring stable phase which has a slightly higher free energy at these compositions. Kinetic factors may be responsible for these discrepancies, that is the inability of the system to nucleate pure A crystallites, perhaps because the composition of the fluid is so different from

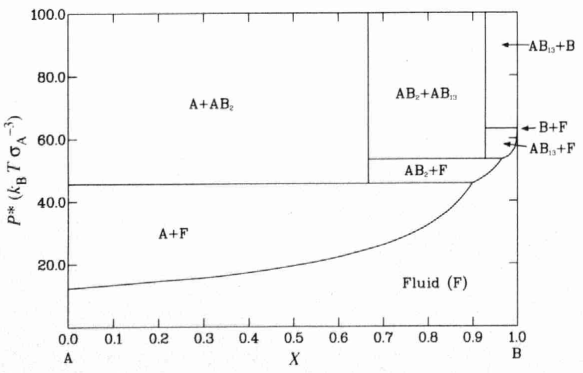

FIG. 2 P–X phase diagram of a binary mixture of hard spheres with a diameter ratio $\alpha = 0.58$. The pressure P^* is given in reduced units $k_B T \sigma_A^{-3}$, where σ_A is the diameter of the large spheres, k_B is the Boltzmann constant, and T is the absolute temperature. In addition to the fluid phase F, we observe the following stable solid phases: pure A, pure B, AB_2 and AB_{13}.

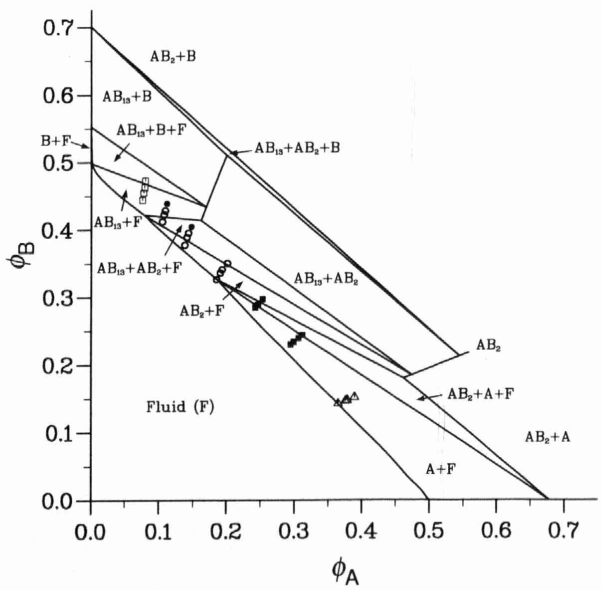

FIG. 3 Phase diagram at constant volume of a binary mixture of hard spheres with a diameter ratio $\alpha = 0.58$. The lines indicate boundaries of two- or three-phase regions. In all cases, the nature of the coexisting phases is indicated. Also shown are the state points studied by Bartlett *et al.*[3] for a binary mixture of colloidal particles with the same diameter ratio. The symbols indicate the phases observed in ref. 3: □, AB_{13} + B + F; ○, AB_{13} + F; ●, AB_{13}; ■, AB_2 + F; △, amorphous solid.

that of the nucleating solid. (We note that in their earlier paper, Bartlett *et al.*[2] did observe formation of pure A from A-rich suspensions at $\alpha = 0.61$; here crystallization was observed for AB_x compositions where x is less than 1.5 and amorphization was observed for larger x.) A similar reasoning could account for the formation of AB_{13} rather than AB_2 at compositions AB_9 and AB_{14}, especially if the interfacial tension between AB_{13} and the fluid were lower than for AB_2. This seems likely in view of the high degree of local icosahedral order in dense fluids. AB_{13} has a particularly large number of icosahedral centres, suggesting that the barrier to nucleation may be particularly low. Detailed examination of its structure shows that all the small (B) atoms are icosahedrally coordinated; the central atom of the cluster is surrounded by a perfect icosahedron of B particles and the B particles on the surface by a distorted icosahedron containing two A particles. □

Received 24 May; acccepted 7 July 1993.

1. Shoemaker, D. P. *et al. Acta crystallogr.* **5,** 637–644 (1952).
2. Bartlett, P., Ottewill, R. H. & Pusey, P. N. *J. chem.* **93,** 1299–1312 (1990).
3. Bartlett, P., Ottewill, R. H. & Pusey, P. N. *Phys. Rev. Lett.* **68,** 3801–3804 (1992).
4. Porter, D. A. & Easterling, K. E. *Phase Transformations in Metals and Alloys* (Chapman & Hall, London, 1992).
5. Murray, M. J. & Sanders, J. V. *Phil. Mag.* **A42,** 721–740 (1980).
6. Barrat, J. L., Baus, M. & Hansen, J. P. *Phys. Rev. Lett.* **56,** 1063–1065 (1986); *J. Phys. C.* **20,** 1413–1430 (1987).
7. Kranendonk, W. G. T. & Frenkel, D. *Molec. Phys.* **72,** 679–697 (1991).
8. Frenkel, D. in *Molecular Dynamics Simulations of Statistical Mechanical Systems: Proc. 97th int. School Phys. 'Enrico Fermi'* (eds Ciccotti, G. & Hoover, W. G.) 151–188 (North-Holland, Amsterdam, 1986).
9. Mansoori, G. A., Carnahan, N. F., Starling, K. E. & Leland, T. W. *J. chem. Phys.* **54,** 1523–1525 (1971).
10. Frenkel, D. & Ladd, A J. C. *J. chem. Phys.* **81,** 3188–3193 (1984).
11. Eldridge, M. D., Madden, P. A. & Frenkel, D. *Molec. Phys.* **79,** 105–120 (1993).
12. Eldridge, M. D. & Madden, P. A., *Molec. Phys.* (in the press).
13. Vos, W. L. *et al. Nature* **358,** 46–48 (1992).
14. Barrat, J. L. & Vos, W. L. *J. chem. Phys.* **97,** 5707–5712 (1992).
15. Loubeyre, P., Jean-Louis, M., LeToullec, R. & Charon-Gérard, L. *Phys. Rev. Lett.* **70,** 178–181 (1993).
16. Hachisu S. & Yoshimura, S. in *Physics of Complex and Supermolecular Fluids* (eds Safran, S. A. & Clark, N. A.) 221–240 (Wiley, New York, 1987).
17. Sanders, J. V. *Phil. Mag.* **A42,** 705–720 (1980).
18. Bartlett, P. *J. Phys.: Condensed Matter* **2,** 4979–4989 (1990).

ACKNOWLEDGEMENTS. We thank P. Bartlett and P. Pusey for discussing their data and the SERC for support.

Stratospheric ozone depletion by $ClONO_2$ photolysis

R. Toumi, R. L. Jones & J. A. Pyle

Centre for Atmospheric Science, Department of Chemistry, University of Cambridge, Lensfield Road, Cambridge CB2 1EW, UK

SPRINGTIME ozone depletion over Antarctica is thought[1,2] to be due to catalytic cycles involving chlorine monoxide, which is formed as a result of reactions on the surface of polar stratospheric clouds (PSCs). When the PSCs evaporate, ClO in the polar air can react with NO_2 to form the reservoir species $ClONO_2$. High concentrations of $ClONO_2$ can also be found at lower latitudes because of direct transport of polar air or mixing of ClO and NO_2 at the edges of the polar vortex. $ClONO_2$ can take part in an ozone-depleting catalytic cycle[18], but the significance of this cycle has not been clear. Here we present model simulations of ozone concentrations from March to May both within the Arctic vortex and at a mid-latitude Northern Hemisphere site. We find increasing ozone loss from March to May. The $ClONO_2$ cycle seems to be responsible for a significant proportion of the simulated ozone loss. An important aspect of this cycle is that it is not as limited as the other chlorine cycles to the timing and location of PSCs; it may therefore play an important role in ozone depletion at warm middle latitudes.

High levels of $ClONO_2$ have been observed in both hemispheres at the edges of the polar winter vortex[3,4] and inside the Arctic spring vortex[5]. We show here for two cases that ozone depletion does not cease once $ClONO_2$ is formed: (1) assuming that at high latitudes (65° N) all the available inorganic chlorine is in the form of $ClONO_2$ after the PSCs have evaporated in March and (2) assuming that this high-latitude air has mixed with air from low latitudes, performing calculations at a lower latitude (55° N). These two cases may be considered representative of air inside and outside the vortex respectively.

The diurnal photochemical box model[6] we use contains a full description of stratospheric chemistry and has been reformulated so that Cl, ClO, Br and BrO are integrated separately. We therefore make no steady-state assumption for Cl + ClO and Br + BrO. The heterogeneous removal of N_2O_5 by the background aerosol layer is also included. Figure 1 shows ozone depletion at an altitude of 19 km (near the peak of the ozone layer) from March to May, assuming different total chlorine and total bromine concentrations[1] that are representative of the years 1980, 1990 and 2000. After 75 days there is a depletion of ozone of 9.5, 12.5 and 16% for these respective years. This is a significant additional change if we consider that models[7] calculate about 20% chemical depletion of ozone from December to March for a 1990 atmosphere. We therefore conclude that there is significant additional ozone depletion months after hererogeneous reactions have ceased. Comparing the 1990 run with the 1980 run shows that ozone is 3.3% lower in 1990, which is about half of the observed column ozone trend for these years[1]. The calculations do not account for mixing and the calculated ozone loss is therefore an upper limit.

The two main ozone depletion cycles are now considered.

$$ClO + BrO \rightarrow Cl + Br + O_2$$

$$Br + O_3 \rightarrow BrO + O_2$$

$$Cl + O_3 \rightarrow ClO + O_2$$

The rate of this catalytic cycle[8] is determined by the reaction ClO + BrO. Ozone can also be destroyed by $ClONO_2$ in the following catalytic cycle.

$$ClONO_2 + h\nu \rightarrow Cl + NO_3 \qquad \alpha = 0.9$$

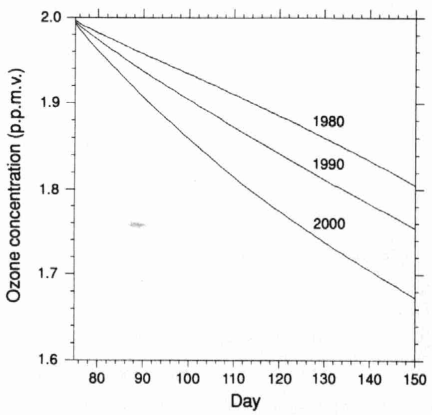

FIG. 1 The concentration of ozone at an altitude of 19 km, 65° N, as a function of time (day 75 = 16 March). Initial (day 74) conditions (in volume mixing ratio) for the years 1980, 1990 and 2000: $ClONO_2 = 2, 3, 4 \times 10^{-9}$; $BrO = 10, 15, 23 \times 10^{-12}$; $HNO_3 = 10, 9, 8 \times 10^{-9}$; for all years: $CH_4 = 0.5 \times 10^{-6}$, $H_2O = 5 \times 10^{-6}$, $H_2 = 0.5 \times 10^{-6}$, $CO = 2 \times 10^{-8}$, $H_2O_2 = 1 \times 10^{-12}$, $ClO = HCl = NO = NO_2 = N_2O_5 = BrONO_2 = CH_3O_2 = 0$, $T = 210$ K, $p = 64.5$ mb. We have specified a rate constant for $N_2O_5(g) + H_2O(l) \rightarrow 2HNO_3(g)$ of 4×10^{-6} s^{-1} on the sulphate aerosol layer[1].